Na+ diffusion kinetics in nanoporous metal-hexacyanoferrates

doi: 10.1039/C5DT03276H

Na^+ diffusion kinetics in nanoporous metal-hexacyanoferrates†

Masamitsu Takachi[a], Yuya Fukuzumi[a] and Yutaka Moritomo*[a,b,c]

Received Xth XXXXXXXXXX 20XX, Accepted Xth XXXXXXXXX 20XX

First published on the web Xth XXXXXXXXXX 200X

DOI: 10.1039/b000000x

Metal-hexacyanoferrates (metal-HCFs) are promising candidates for cathode materials of sodium-ion secondary batteries (SIBs). Here, we systematically investigated Na^+ diffusion constants (D) and their activation energies (E_a) in metal-HCFs against the framework size (= a/2). We found that the magnitude of D (E_a) systematically increases (decreases) with increases in a, indicating that steric hindrance plays a dominant role in Na^+ diffusion.

Coordination polymers are promising cathode materials for SIBs, due to their robust nature of their three-dimensional (3D) frameworks against Na^+ intercalation/deintercalation. Among the coordination polymers, metal-HCFs, $Na_xM[Fe(CN)_6]_y$ (M is metal element), are most intensively investigated as cathode materials for SIBs.[1–10] The compounds show 3D jungle-gym-type framework with periodic cubic nanopores, 0.5 nm at the edge.[11] Significantly, the framework size (= a/2) is finely-controlled by the substitution of M. Actually, in $(Cs,Rb)_xM^{II}[Fe^{III}(CN)_6]_y$ (M = Co, Fe, Ni, Cu, Zn, Mn, and Cd), a increases linearly with increase in the ionic radius (r) of M as a [Å] = 0.8091 + 2r [Å].[11,12]

The electrochemical performance of the metal-HCF family has been rapidly improved every year. Goodenough's group[1] have reported Na^+ intercalation behaviors in a K-M-Fe(CN)$_6$ system (M = Mn, Fe, Co, No, Cu, Zn), even though their Coulomb efficiency is very low. The Coulomb efficiency is significantly improved in thin films of $Na_{1.32}Mn^{II}[Fe^{II}(CN)_6]_{0.83}3.5H_2O$,[2] and $Na_{1.6}Co^{II}[Fe^{II}(CN)_6]_{0.9}2.9H_2O$:[3] the films show high capacities of 109 and 135 mAh/g and average operating voltages of 3,4 and 3.6 V against Na, respectively. By a structural optimization, Yang *et al.*[5] demonstrated that $Na_{1.76}Ni_{0.12}Mn_{0.88}[Fe(CN)_6]_{0.98}$ exhibits an excellent cycle life with a capacity of 118 mAh/g. In addition, Lee *et al.*[6] reported that $Na_2Mn^{II}[Mn^{II}(CN)_6]$ show a huge capacity of 209 mAh/g mediated by one- and two-electron reactions per a chemical formula. Significantly, the metal-HCF also works as cathode materials of lithium-ion secondary batteries (LIBs).[13–17] Then, we can directly compare the diffusion dynamics of Li^+ (r = 0.92 Å) and Na^+ (r = 1.18 Å) within the same the host framework.

In this Communication, we investigated the framework size dependence of Na^+ diffusion constants (D) and their activation energies (E_a) in metal-HCFs. We found that the magnitude of D (E_a) systematically increases (decreases) with increases in the framework size. We further compare the diffusion dynamics of Na^+ and Li^+ within the same Mn-HCF and Cd-HCF frameworks. Reflecting the smaller ionic radius, the diffusion constant of Li^+ is much higher than that of Na^+.

Films of Co-, Mn- and Cd-HCF were fabricated by the electrochemical deposition on an indium tin oxide (ITO) transparent electrodes under potentiostatic conditions at - 0.45 V vs. a standard Ag/AgCl electrode.[14,18] The electrolytes were aqueous solutions containing 0.8mM $K_3[Fe^{III}(CN)_6]$, 0.5mM $Co^{II}(NO_3)_2$, and 5M $NaNO_3$ for Co-HCF, that containing 1.0mM $K_3[Fe^{III}(CN)_6]$, 1.5mM $Mn^{II}Cl_2$, and 1M NaCl for Mn-HCF, and that containing 1.0mM $K_3[Fe^{III}(CN)_6]$, 1.5mM $Cd^{II}Cl_2$, and 1M NaCl for Cd-HCF. The obtained film was transparent with a thickness (d) of $\approx$ 500 nm (Fig. S1). Chemical composition of the Co-HCF film determined to be $Na_{1.52}Co^{II}[Fe^{II}(CN)_6]_{0.88}3.1H_2O$ (denoted as CoF88) using the inductively coupled plasma (ICP) method and a CHN organic elementary analyzer. Calcd: Na, 10.4; Co, 17.6; Fe, 14.6; C, 18.9; H, 1.8; N, 22.0%. Found: Na, 11.2; Co, 17.4; Fe, 15.3; C, 18.5; H, 1.9; N, 20.0%. Chemical composition of the Mn-HCF film determined to be $Na_{1.36}Mn^{II}[Fe^{II}(CN)_6]_{0.84}3.4H_2O$ (MnF84). Calcd: Na, 9.7; Mn, 16.9; Fe, 14.5; C, 18.7; H, 2.1; N, 21.8%. Found: Na, 10.6; Mn, 16.8; Fe, 14.7; C, 18.2; H, 2.1; N, 20.9%. Chemical composition of the Cd-HCF film determined to be $Na_{1.76}Cd^{II}[Fe^{II}(CN)_6]_{0.94}3.8H_2O$ (CdF94). Calcd: Na, 9.6; Cd, 26.8; Fe, 12.5; C, 16.1; H, 1.9; N, 18.8%. Found: Na, 10.3; Cd, 27.0; Fe, 13.1; C, 15.8; H, 1.8; N, 17.9%. The X-ray powder diffraction (XRD) patterns of the CoF88, MnF84, and CdF94 films were obtained with use of a synchrotron-

† Electronic Supplementary Information (ESI) available: [details of any supplementary information available should be included here]. See DOI: 10.1039/b000000x/

[a] *Graduate School of Pure & Applied Science, University of Tsukuba, Tennodai 1-1-1, Tsukuba, Ibaraki 305-7571, Japan. E-mail: moritomo.yutaka.gf@u.tsukba.ac.jp*

[b] *Faculty of Pure & Applied Science, University of Tsukuba, Tennodai 1-1-1, Tsukuba, Ibaraki 305-7571, Japan.*

[c] *Center for Integrated Research in Fundamental Science and Engineering (CiRfSE), University of Tsukuba, Tsukuba, Ibaraki 305-8571, Japan*

radiation X-ray source (Fig. S2). The crystal structure was hexagonal (R$\underline{3}$m; Z = 12) for MnF84 and CoF88 white it is face-centered cubic (Fm$\underline{3}$m; Z = 4) for CdF94. The masses of the films were measured using a conventional electronic weighing machine by subtracting the mass of the substrate.

In order to investigated the Na^+diffusion kinetics, electrochemical impedance spectra (EISs) were measured with a potentiostat (BioLogic SP-150) in a two-pole beaker type cell against Na metal. The electrolyte is propylene carbonate (PC) containing 1M $NaClO_4$. The active area of the film was 1 cm^2. The frequency range was from 5 mHz to 200 kHz, and the amplitude was 30 mV. The concentration (x) of Na^+ was controlled by charge/discharge process of the battery cell. The magnitudes of x was evaluated by the relative charge with assuming the ideal redox reaction. In the MnF84 and CoF88 films, the discharge curve shows a characteristic two-plateau[2–4] (Fig. S3). The high- and low-V plateaus of MnF84 are ascribed to $1.36Na^+ + Mn^{II}_{0.48}Mn^{III}_{0.52}[Fe^{III}(CN)_6]_{0.84} \rightarrow 0.84Na^+ + Na_{0.52}Mn^{II}[Fe^{III}(CN)_6]_{0.84}$ and $0.84Na^+ + Na_{0.52}Mn^{II}[Fe^{III}(CN)_6]_{0.84} \rightarrow Na_{1.36}Mn^{II}[Fe^{II}(CN)_6]_{0.84}$, respectively. The high- and low-V plateaus of CoF88 are ascribed to $1.52Na^+ + Co^{III}[Fe^{III}(CN)_6]_{0.52}[Fe^{II}(CN)_6]_{0.36} \rightarrow Na^+ + Na_{0.52}Co^{III}[Fe^{II}(CN)_6]_{0.88}$ and $Na^+ + Na_{0.52}Co^{III}[Fe^{II}(CN)_6]_{0.88} \rightarrow Na_{1.52}Co^{II}[Fe^{II}(CN)_6]_{0.88}$, respectively. In the high-V plateau, the EISs are too deformed to analyze (Fig. S4). So, we chose x [= 0.6 (0.8) for MnF84 (CoF88)] at the central region of the low-V plateau. In the CdF94, the discharge curve shows a single-plateau[18] (Fig. S3): $0.94Na^+ + Na_{0.82}Cd^{II}[Fe^{III}(CN)_6]_{0.94} \rightarrow Na_{1.76}Cd^{II}[Fe^{II}(CN)_6]_{0.94}$. We chose x (= 0.5) at the central region of the plateau.

The formal valences at the EIS measurements are $Na_{0.6}Mn^{II}[Fe^{II}(CN)_6]_{0.08}[Fe^{III}(CN)_6]_{0.76}$ (MnF84), $Na_{0.8}Co^{II}{}_{0.28}Co^{III}{}_{0.72}[Fe^{II}(CN)_6]_{0.88}$ (CoF88), and $Na_{1.1}Cd^{II}[Fe^{II}(CN)_6]_{0.28}[Fe^{III}(CN)_6]_{0.66}$ (CdF94). We note that the molar ratios of the divalent metals (Mn^{II}, Fe^{II}, Co^{II}, and Cd^{II}) and the heavy metals (Mn, Fe, Co, and Cd) are close to each other: 0.59, 0.61, and 0.66 for MnF84 (x = 0.6), CoF88 (0.8), and CdF94 (1.1), respectively. In other words, the electrostatic forces between Na^+ and the host frameworks are nearly the same. In addition, the hexagonal distortion of the as-grown MnF84 (x =1.36) and CoF88 (1.52) disappears with decrease in x.[2–4] Actually, crystal structures are face-centered cubic (Fm$\underline{3}$m; Z = 4) at the EIS measurements: a = 10.56 Å for MnF84 (x = 0.6) and 9.97 Å for CoF88 (0.8). Thus, metal-HCFs give us nice platforms to investigated the interrelation between the Na^+ diffusion kinetics and the framework size.

Figure 1(a) shows EISs of CoF88, MnF84, and CdF94 films against Na. In the high frequency region, the spectra show semicircles. With increase in the frequency (f), the spectra show straight lines with the angle of $\sim \pi/4$ against the imaginary axis [broken straight lines in Fig. 1(a)]. With further decreases in f, the data deviates from the broken line. We define the critical frequency (f_c) where the data begins to deviate from the broken line. Then, f_c^{-1} is the characteristic time when the diffusion length of Na^+ reaches the film thickness (d). The diffusion constant (D) is expressed as $D = 2\pi f_c d^2$. Looking at Fig. 1(a), we found that f_c in the CoF88 film is much smaller than those in the MnF84 and CdF94 films.

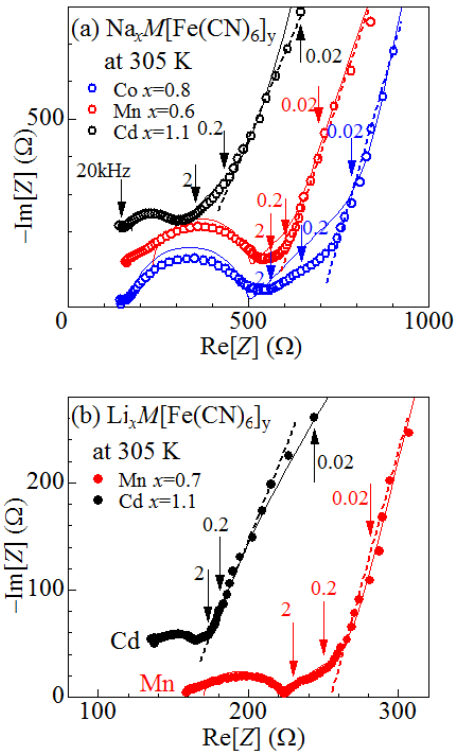

Fig. 1: (a) EISs of CoF88, MnF84, and CdF94 films in PC containing 1M $NaClO_4$ at 305 K. (b) EISs of the Li-substituted MnF84 and CdF94 film in EC / DEC containing 1M $LiClO_4$ at 305 K. Arrows indicate the frequencies. Broken straight lines are eye-guided ones. Solid curves are results of the least-squares fittings with the Randles equivalent circuit model (see text).

We quantitatively analyzed the EISs with a Randles equivalent circuit model, which consists of the high frequency resistance (R_0) of electrolyte, ionic charge-transfer resistance (R_{ct}), double layer capacitance (C_{dl}), and restricted diffusion impedance ($R_d \cdot z_d$: R_d and z_d are characteristic resistance and reduced diffusion impedance, respectively) of flat plate with thickness d.[19] In order to reproduced the finite slope in the low frequency region, we used the constant phase element (CPE)-restricted form as z_d:[20]

$$z_d(u) = \frac{\alpha u^n + \sqrt{u}\coth\sqrt{u}}{u + \alpha u^{n+1/2}\coth\sqrt{u}}, u = i\frac{\omega d^2}{D}, \quad (1)$$

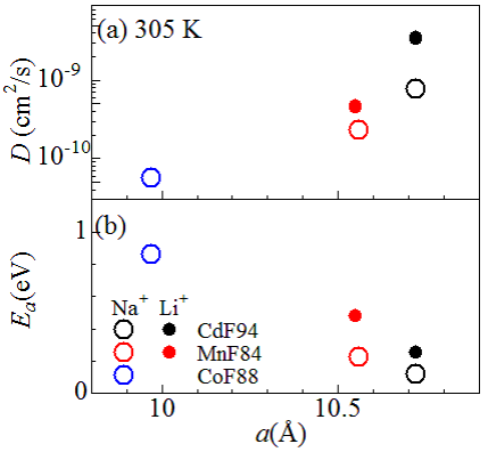

Fig. 2: (a) Diffusion constant (D) and (b) activation energy (E_a) in CoF88, MnF84, and CdF94 films against lattice constant (a). Open and closed circles stand for Na^+ and Li^+, respectively.

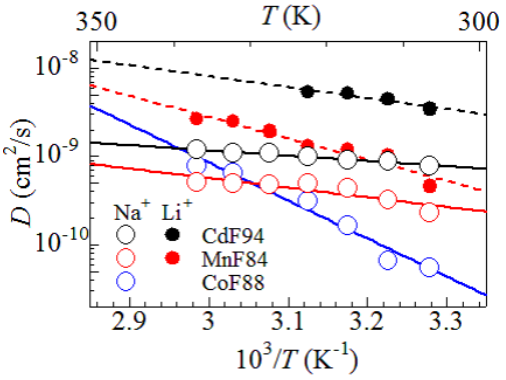

Fig. 3: Arrenius plot of diffusion constant (D) in CoF88, MnF84, and CdF94 films. Open and closed circles stand for Na^+ and Li^+, respectively. Solid lines are results of least-squares fitting.

where ω (= $2\pi f$), α, n is the angular velocity, dimensionless quantity, and specific exponent, respectively. We evaluated seven parameters, *i.e.*, R_0, R_{ct}, C_{dl}, R_d, α, n, and D, by least-squares fittings of the EIS curves [solid curves in Fig. 1(a)].

We further investigated the diffusion kinetics of Li^+ in the same host framework. We measured the EISs in ethylene carbonate (EC) / diethyl carbonate (DEC) containing 1M $LiClO_4$ against Li metal. Before the measurements, Na^+ of the films is electrochemically substituted for Li^+. The concentration (x) of alkali cations was controlled by charge/discharge process of the battery cell. The magnitudes of x was evaluated by the relative charge with assuming the ideal redox reaction[18]. In the MnF84 films, the discharge curve shows a characteristic two-plateau structure[13] (Fig. S5). Figure 1(b) shows EISs of MnF84 and CdF94 films against Li. We evaluated the D values by least-squares fittings of the EIS curves with the Randles equivalent circuit model [solid curve in Fig. 1(b)].

In Fig. 2(a), we plotted D against a. Open and closed circles stand for Na^+ and Li^+, respectively. The magnitudes of a were evaluated with use of the x dependence of a reported in literature.[4,18] For CdF94, we used the structural data of the Li-substituted Cd-HCF.[18] We found that the Na^+ diffusion constant steeply increases with increase in a: D = 0.5×10^{-10}, 2.3×10^{-10}, and 7.7×10^{-10} cm^2/s at a = 9.97 (CoF88), 10.56 (MnF84), and 10.70 Å (CdF94), respectively. This behavior is reasonable because the wider the framework becomes the faster the guest ion transfer to the adjacent cubic nanopore. We further found that the diffusion constant of the smaller Li^+ is much higher than that of Na^+ diffusion constant in the same MnF84 and CdF94 framework.

In order to evaluate the activation energy (E_a) of D, we investigated temperature dependence of EISs (Figs. S6 and S7) for CoF88, MnF84, and CdF94 films. The D values were evaluated by the least-squares fittings of the EIS curves with the Randles equivalent circuit model [solid curve in Figs. S6 and S7]. Figure 3 shows temperature dependence of D. As indicated by least-squares fitted straight lines, D obeys the thermal-activation law: $D \propto \exp(-E_a/k_BT)$. In Fig. 2(b), we plotted E_a against a. We found that E_a steeply decreases with increases in a. The activation energy corresponds to the barrier height of the Na^+ potential curve along the ion migration path. An *ab initio* calculation[12] indicates that the potential shows local maximum at the window position between the neighboring cubic nanopores. Then, the suppressed E_a in the large-a compound is ascribed to the weaker guest-host interaction, and resultant lower potential barrier at the window position.

Finally, let us discuss the effects of the Na^+ - H_2O and Na^+ - Na^+ interactions on D. The metal-HCF has two types of crystal waters, *i.e.*, the ligand and zeolite waters, in addition to Na^+. Among them, the zeolite waters occupy the nanopores and disturb the Na^+ diffusion. In other words, the Na^+ - H_2O interaction is expected to suppress D with increase in the number (n_z) of the zeolite water. The actual D value, however, increases with increase in n_z: n_z = 2.4, 2.4, 3.4 for CoF88, MnF84, CdF94, respectively. This indicates that the Na^+ - H_2O interaction has minor effect on D. The Na^+ - Na^+ interaction is also expected to suppress D with x, because Na^+ cannot hop to the occupied adjacent site. We, however, found that the D value of the MnF84 film is less sensitive to x: D = 2.3×10^{-10}, 2.2×10^{-10}, and 2.6×10^{-10} cm^2/s at x = 0.6, 0.9, and 1.1, respectively.

In conclusion, we demonstrate that diffusion kinetics of alkali cations in metal-HCFs crucially depends on not only the ionic radius but also the framework size. The high Na^+ diffusion constant ($\approx 10^{-9}$ cm^2/s) in the wide framework compounds suggests that metal-HCFs are promising cathode materials of SIBs.

This work was supported by the Mitsubishi Foundation, Yazaki Memorial Foundation, and Nippon Sheet Glass Foundation. The elementary analyses were performed at the Chemical Analysis Division, Research Facility Center for Science and Engineering, University of Tsukuba. The XRD measurements were performed under the approval of the Photon Factory Program Advisory Committee (Proposal No. 2014G507).

References

1 Y. Lu, L. Wang, J. Cheng, and J. B. Goodenough, Chem. Commun., 2012, **48**, 6544.
2 T, Matsuda, M. Takachi, and Y. Moritomo, Chem. Commun., 2013, **49**, 2750.
3 M. Takachi, T. Matsuda, and Y. Moritomo, Appl. Phys. Express, 2013, **6** 025802.
4 M. Takachi, T. Matsuda, and Y. Moritomo, Jpn. J. Appl. Phys., 2014, **53** 067101.
5 D. Yang, J. Xu, X.-Z. Liao, Y.-S. He, H. Liu, and Z.-F. Ma, Chem. Commum., 2014, **50**, 13377.
6 H. W. Lee, R. Y. Wang, M. Oasta, S. W. Lee, N. Liu, Y. Chi, Nature Commun., 2014, **5**, 5280.
7 L. Wang, J. Song, R. Qiao, L. A, Wray, M. A. Hossain, Y.-D. Chung, W. Yang, Y. Lu, D. Evans, J.-J. Lee, S. Vail, X. Zhao, M. Nishijima, S. Kakimoto, and J. B. Goodenough, J. Am. Chem. Soc., 2015, **137**, 2548.
8 S. Yu, Y. Li, Y. Lu, B. Xu, Q. Wang, M. Yan, and Y. Jing, J. Power Sources, 2015, **275**, 45.
9 Y. You, X.-L. Wu, Y.-X. Yin, and Y,-G. Guo, Energy Environ. Sci., 2014, **7**, 1643.
10 L. Wang, Y. Lu, J. Liu, M. Xu, J. Cheng, D. Zhang and J. B. Goodenough, J. B. Angew. Chem., 2013, **52**, 1964.
11 T. Matsuda, J. E. Kim, Y. Moritomo, Phys. Rev. B, 2009, **79**, 172302.
12 Y. Moritomo and H. Tanaka, Adv. Cond. Mat. Phys., 2013, **2013**, Article ID 539620.
13 T. Matsuda and Y. Moritomo, Appl. Phys. Express, 2011, **4**, 047101.
14 M. Takachi, T. Matsuda and Y. Moritomo, Jpn. J. Appl. Phys., 2013, **52**, 044301.
15 S. Yagi, M. Fukuda, R. Makiura, T. Ichitsubo, and E. Matsubara, J. Mater. Chem. A, 2013, **2**, 8041.
16 Y. Mizuno, M. Okubo, E. Hosono, T. Kudo, H. Zhou, K. Ohishi, J. Phys. Chem. C, 2013, **117**, 10877.
17 M. Okubo, D. Asakura, Y. Mizuno, J.-D. Kim, T. Mizokawa, T. Kudo, I. Honma, J. Phys. Chem. Lett., 2010, **1**, 2063.
18 Y. Moritomo, M. Takachi, Y. Kurihara, and T. Matsuda, Appl. Phys. Express, 2012, **5**, 041801.
19 T. Shibata, Y. Fukuzumi, W. Kobayashi, and Y. Moritomo, Scientific Reports, 2015, **5**, 90006.
20 J. Bisquert, G, Garcia-Belmonte, F. Fabregat-Santiago, and P. R. Bueno, J. Electroanal. Chem., 1999, **475**, 152.